

Dynamics of an ultra-strongly-coupled system interacting with a driven nonlinear resonator

Suguru Endo,¹ Yuichiro Matsuzaki,² Kosuke Kakuyanagi,² Shiro Saito,² Neill Lambert,¹ and Franco Nori^{1,3}

¹*CEMS, RIKEN, 351-0198 Wako-shi, Japan*

²*NTT Basic Research Laboratories, NTT Corporation, 3-1 Morinosato-Wakamiya, Atsugi, Kanagawa, 243-0198, Japan.*

³*Department of Physics, The University of Michigan, Ann Arbor, MI 48109-1040, USA*

In the ultra-strong coupling regime of a light-matter system, the ground state exhibits non-trivial entanglement between the atom and photons. For the purposes of exploring the measurement and control of this ground state, here we analyze the dynamics of such an ultra-strongly-coupled system interacting with a driven nonlinear resonator acting as a measurement apparatus. Interestingly, although the coupling between the atom and the nonlinear resonator is much smaller than the typical energy scales of the ultra-strongly-coupled system, we show that we can generate a strong correlation between the nonlinear resonator and the light-matter system. A subsequent coarse-grained measurement on the nonlinear resonator significantly affects the light-matter system, and the phase of the light changes depending on the measurement results. Also, we investigate the conditions for when the nonlinear resonator can be entangled with the ultra-strongly coupled system, which is the mechanism that allows us to project the ground state of the ultra-strongly coupled system into a non-energy eigenstate.

PACS numbers:

The hybridization of light and matter is one of the core topics in quantum physics, and has been the focus of many theoretical and experimental efforts [1–3, 5? – 7]. In this context, it is expected that if the coupling strength between light and matter becomes extremely strong, so that it surpasses the light resonance frequency, it is predicted that a new ground state will emerge [8–11]. This regime, called the deep-strong coupling regime, contains a range of unique phenomena, such as large ground-state entanglement [8], a long-lived effective qubit memory [12, 13], and quantum phase transitions [14].

This regime was recently experimentally demonstrated [15–17]. However, a remaining challenge in this regime regards the implementation of arbitrary measurement and control of the hybridized system. Measurements of ultra-strongly-coupled systems so far have mostly focused on extraction of photons from the ground state, via modulation of some system parameter [18] (akin to approaches used to observe the dynamical Casimir effect [19–23]), or transitions out of the ground-state itself [24, 25]. Proposals for QND measurements of the ground-state with minimal backaction have also recently been explored theoretically [26, 27]. Projective measurements in an arbitrary basis would significantly broaden the possibilities of controlling these highly quantum states.

Since the ground state of the ultra-strongly-coupled system contains virtual photons, we can also in principle extract the virtual photons if the state is projected into a non-energy eigenbasis state. In this case, a correlation between the phase of the extracted photons and the measurement results occurs, which cannot be observed by unitary operations. Moreover, non-eigenbasis measurements on a ground state of a ultra-strongly-coupled system could potentially be used to induce an optical cat state, which is itself a resource for quantum information processing [12, 13]. Given these potential benefits,

it is important to investigate the interaction between an ultra-strongly-coupled system and a measurement apparatus capable of realizing non-eigenbasis measurements [28–30]. Although there are several previous works studying the quantum properties of the ground state in an ultra-strongly coupled system [8–11], here we focus on how to perform non-energy eigenbasis measurements on the ground state of such a system.

In this paper, we analyze the dynamics of an ultra-strongly coupled system interacting with a measurement apparatus. Although there are some theoretical proposals to use a detector that continuously monitors the system [29], we consider a binary-outcome measurement after the interaction with the target qubit, which is considered to induce a strong correlation with the target qubit [31, 32]. While linear resonators have been used as a standard method for quantum measurement in cavity quantum electrodynamics and circuit quantum electrodynamics, in some cases a nonlinearity has been employed to improve qubit readout [31, 33–37]. Due to the bifurcation effect, the state of the nonlinear resonator becomes highly sensitive to the state of the matter qubit, which enables one to implement a high-visibility readout.

Here, with both full numerical modeling and a low-energy approximation, we investigate how the driven nonlinear resonator interacts with the ultra-strongly-coupled system. Surprisingly, although the coupling between the nonlinear measurement device and the ultra-strongly-coupled system is almost negligible, we show that the dynamic evolution can induce a strong correlation between them. Moreover, we evaluate how much entanglement and quantum discord is generated between system and measurement device during this evolution.

The remainder of this paper is organized as follows. First, we introduce the ultra-strongly-coupled system and its ground state. Second, we discuss the interaction

between the nonlinear resonator and the ultra-strongly-coupled system, and we introduce a coarse-graining measurement of the nonlinear resonator itself. Third, we present numerical results to show how a strong correlation arises, even in a parameter regime where the coupling strength may be incorrectly considered to be negligible. Fourth, we show that, as the effective energy of the ultra-strongly-coupled system decreases, the entanglement between the ultra-strongly coupled system and the nonlinear resonator-increases. Finally, we examine the quantum discord between the ultra-strongly coupled system and the nonlinear resonator.

I. ULTRA-STRONG COUPLING BETWEEN LIGHT AND MATTER

The Hamiltonian of light in a single-mode cavity ultra-strongly-coupled to matter (where the matter is well described by a two-level system) is, in its simplest form, given by the Rabi model [38]

$$\hat{H}_{\text{Rabi}} = \frac{\omega_q}{2} \hat{\sigma}_x + g(\hat{a} + \hat{a}^\dagger) \hat{\sigma}_z + \omega_r \hat{a}^\dagger \hat{a}, \quad (1)$$

where \hat{a} (\hat{a}^\dagger) is an annihilation (creation) operator for the single-mode cavity/resonator, ω_q (ω_r) denotes the qubit (resonator) frequency, and g is the coupling strength between resonator (light) and qubit (matter).

It is worth mentioning that, when the matter is in the form of a superconducting flux qubit, as in the recent ultra-strong coupling experiment in [15], $\hat{\sigma}_z = |L\rangle\langle L| - |R\rangle\langle R|$ is diagonal in the persistent-current basis of L and R of the superconducting flux qubit.

Throughout this paper we assume that the qubit frequency is much smaller than the resonator frequency, allowing us later to use an adiabatic approximation. In this case, in the limit $\omega_q \rightarrow 0$, we can approximately write the ground state of this system as [8, 9, 11]

$$|G\rangle \simeq \frac{1}{\sqrt{2}}(|R\rangle|\alpha\rangle - |L\rangle|-\alpha\rangle) \quad (2)$$

where

$$\alpha = g/\omega_r, \quad (3)$$

is the ratio of the coupling strength and resonator energy. As an example, using parameters close to those used in [15], we plot the Q function of the reduced density matrix of $|G\rangle$ where the atom is traced out in Fig.1. The definition of the Q function for a state $\hat{\rho}$ is $Q(\beta) = \frac{1}{\pi} \langle \beta | \hat{\rho} | \beta \rangle$, where $|\beta\rangle$ is a coherent state for a complex number β . We plot the real part of the β in the x axis while we plot the imaginary part of the β in the y axis. It is worth mentioning that, if we can realize a projective measurement in the basis of $\frac{1}{\sqrt{2}}(|R\rangle + |L\rangle)$ or $\frac{1}{\sqrt{2}}(|R\rangle - |L\rangle)$ on this ground state, we can create an optical cat state, $\frac{1}{\sqrt{2}}(|\alpha\rangle + |-\alpha\rangle)$, in the cavity.

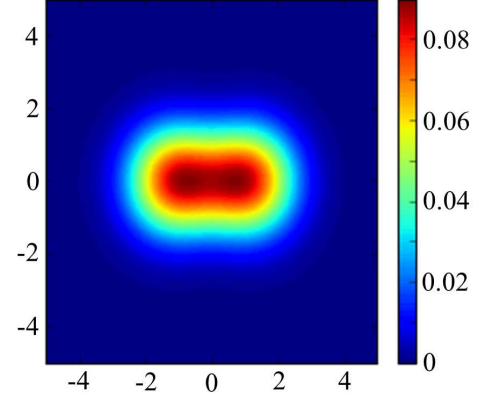


FIG. 1: (Color online) The Q function of the reduced density matrix of the cavity in the ground state $|G\rangle$. Here $\omega_q = 2\pi \times 0.299$ GHz, $g = 2\pi \times 4.920$ GHz, $\omega_r = 2\pi \times 6.336$ GHz.

II. USING A NONLINEAR RESONATOR AS A MEASUREMENT DEVICE

Here, as a measurement apparatus, we consider a driven nonlinear resonator dispersively coupled to the qubit. It is well understood that a nonlinear resonator can exhibit a bistability [39–43], which makes such a device sensitive to small changes in external fields. In addition, the nonlinearity induces a rapid change in the photon number under driving [40], compared to the linear case. When used as a measurement device the fast evolution and the sensitivity of the steady-state to weak fields results in a strong and fast correlation of the nonlinear resonator state with the qubit being measured, potentially giving a means to implement a rapid projective measurement. One should note that typically the state of the nonlinear resonator is itself measured by standard homodyne techniques [38], and this measurement provides the information about the qubit state.

It is worth mentioning that there are some theoretical proposals to treat such a measurement device as a two level system when the measurement outcomes are binary [28]. However, since such a simplification cannot quantify the strength of the correlation between the target qubit and measurement apparatus during the measurement process, we need to model the measurement apparatus with a proper Hamiltonian as we will describe below.

The total system, composed of the ultra-strongly-coupled light-matter system, and the nonlinear resonator measurement device, can be described by the Hamiltonian [8, 10, 11, 40–43]

$$\hat{H}_{\text{tot}} = \hat{H}_{\text{Rabi}} + \hat{H}_{\text{nr}} + \hat{H}_{\text{int}} \quad (4)$$

$$\hat{H}_{\text{nr}} = \delta \hat{b}^\dagger \hat{b} - \chi (\hat{b}^\dagger \hat{b})^2 - \frac{f}{2} (\hat{b} + \hat{b}^\dagger) \quad (5)$$

$$\hat{H}_{\text{int}} = J \hat{\sigma}_z \hat{b}^\dagger \hat{b}, \quad (6)$$

where \hat{b} is an annihilation operator of the nonlinear sys-

tem, δ denotes the detuning between the nonlinear resonator energy and driving frequency, χ denotes the nonlinearity strength, and f denotes the driving strength of the nonlinear resonator. In addition, J is the coupling between the qubit and the nonlinear resonator. In order to include the loss of photons from the nonlinear resonator, we adopt the following Lindblad master equation, valid when the coupling between nonlinear resonator and its environment is weak, and when the coupling J between nonlinear resonator and qubit is weak [40–43]

$$\frac{d}{dt}\hat{\rho} = -i[\hat{H}_{\text{tot}}, \hat{\rho}] + \frac{\kappa}{2}(2b\hat{\rho}b^\dagger - \hat{b}^\dagger\hat{b}\hat{\rho} - \hat{\rho}\hat{b}^\dagger\hat{b}), \quad (7)$$

where κ denotes the photon leakage rate from the nonlinear cavity. The potential losses from the ultra-strongly coupled system are described later.

A. Coarse-graining of the measurement outcome

After the qubit and the measurement apparatus have interacted for some time, we need to implement a measurement on the measurement apparatus itself. Ideally, one could apply a projection operator $\hat{P}_x = |x\rangle\langle x|$ on the nonlinear resonator, where $|x\rangle$ is an eigenvector of the quadrature operator $\hat{x} = (\hat{b} + \hat{b}^\dagger)/2$. However, due to imperfections in the measurement setup, one cannot resolve arbitrarily small differences in the state of the resonator. Normally, to describe more realistically the measurement process, one takes this into account by considering the integrated signal-to-noise [44], where the noise can include contributions from vacuum fluctuations and noise in the measurement apparatus itself. Here, instead we employ a “coarse graining” approximation described by the following operator

$$\hat{E}_x = \frac{1}{\pi^{1/4}\sqrt{2\sigma}} \int_{-\infty}^{\infty} dx' \exp\left[-\frac{(x' - x)^2}{4\sigma^2}\right] |x'\rangle\langle x'|, \quad (8)$$

where σ is the width of the error of the measurement process, and the post-measurement state is described by $\hat{E}_x\hat{\rho}\hat{E}_x/\text{Tr}[\hat{E}_x\hat{\rho}\hat{E}_x]$. This approach allows us to consider the transition from small to large noise situations without being specific about the source of the noise.

Correlations between the nonlinear resonator and the qubit should occur after they have interacted for some time, and, for the parameter regime we use in this work, typically the nonlinear resonator state with $x \geq 0$ ($x < 0$) corresponds to an outcome where the qubit was initially in its excited (ground) state. We can describe the post measurement state of the ultra-strongly-coupled (USC) system as

$$\hat{\rho}_{x \geq 0} = \frac{1}{N} \int_{-\infty}^{\infty} dx \text{erfc}\left(-\frac{x}{\sqrt{2\sigma}}\right) \langle x | \hat{\rho} | x \rangle \quad (9)$$

$$\hat{\rho}_{x < 0} = \frac{1}{N'} \int_{-\infty}^{\infty} dx \text{erfc}\left(\frac{x}{\sqrt{2\sigma}}\right) \langle x | \hat{\rho} | x \rangle, \quad (10)$$

where erfc is the complementary error function and N and N' are normalization factors.

In the limit when $\sigma \rightarrow +\infty$, we obtain $\hat{\rho}_{x \geq 0} = \hat{\rho}_{x < 0} \propto \int_{-\infty}^{\infty} dx \langle x | \hat{\rho} | x \rangle$. In this case, the measurement results do not contain any information of the post-measurement state of the qubit. On the other hand, we obtain

$$\hat{\rho}_{x \geq 0} \propto \int_0^{\infty} dx \langle x | \hat{\rho} | x \rangle, \quad (11)$$

and

$$\hat{\rho}_{x < 0} \propto \int_{-\infty}^0 dx \langle x | \hat{\rho} | x \rangle, \quad (12)$$

in the limit $\sigma \rightarrow 0$, which corresponds to an ideal projective measurement that can perfectly distinguish $x \geq 0$ or $x < 0$.

B. Ultra-strongly coupled system losses

We must also consider the coupling between the cavity component of the ultra-strongly-coupled system and its environment. This allows us to evaluate properties of the photons leaking out from the system after the measurement on the nonlinear resonator. The interaction Hamiltonian between the system and the environment can be described as [44]

$$\hat{H}_I = \int d\omega \kappa(\omega) (\hat{a} + \hat{a}^\dagger)(\hat{c}(\omega) + \hat{c}(\omega)^\dagger) \quad (13)$$

, where $\hat{c}(\omega)$ denotes a boson annihilation operator for the environment (e.g., an open transmission line). When we move to the Heisenberg picture, defined by the Hamiltonian \hat{H}_{Rabi} , the operator $(\hat{a} + \hat{a}^\dagger)$ becomes time dependent. We can define $(\hat{a} + \hat{a}^\dagger)(t) = \hat{X}^+ + \hat{X}^-$, where \hat{X}^+ (\hat{X}^-) denotes the positive (negative) frequency component [45–47]. With a rotating wave approximation, we have

$$\hat{H}_I \approx \kappa(\omega) [\hat{X}^+ \hat{c}(\omega)^\dagger + \hat{X}^- \hat{c}(\omega)]. \quad (14)$$

By using a Markov approximation $\kappa(\omega) = \sqrt{\gamma/2\pi}$ with the standard input-output formalism [44], we obtain

$$\hat{c}_{\text{out}} = \hat{c}_{\text{in}} + \sqrt{\gamma} \hat{X}^+ \quad (15)$$

$$\hat{c}_{\text{in}} \equiv \frac{1}{\sqrt{2\pi}} \int d\omega e^{-i\omega t} \hat{c}(\omega), \quad (16)$$

where \hat{c}_{out} (\hat{c}_{in}) denotes an output (input) operator. This means that the photons leaking from the USC system into the transmission line are described by the operators \hat{X}^+ and \hat{X}^- . We use these definitions to describe the potentially observable real photons in the USC system. However, in the simulations we perform, we assume that the decay time of the USC system is longer than all other time scales that we consider, and so we only explicitly take into account the decay of the nonlinear measurement apparatus.

III. FULL DYNAMICS OF THE USC SYSTEM AND NONLINEAR MEASUREMENT DEVICE

Using the parameters from [15], we numerically [48, 49] solve Eq. (7), with the USC system in the initial state $|G\rangle$, and we consider the post-measurement state of the USC system after the coarse-graining measurement on the nonlinear resonator is performed at the time $t = 500$ ns. In Fig. (2), we show how the Q function of the resonator of the USC system depends on the coarse-graining value. One immediately sees a change in the state of the USC resonator when the measurement becomes weaker (corresponding to an increase of the coarse-graining values of σ).

In Figs. 3 and 4 we plot the post-measurement observable photons in the USC cavity, $\hat{x}' = (\hat{X}^+ + \hat{X}^-)/2$ and the state of the qubit $\hat{\sigma}_z = |L\rangle\langle L| - |R\rangle\langle R|$, for $\hat{\rho}_{x \geq 0}$ and $\hat{\rho}_{x < 0}$. For comparison, we consider both a linear resonator ($\chi = 0$) and a nonlinear resonator ($\chi \neq 0$) as the measurement devices. In addition, in Fig. 5, we show the average photon number inside the measurement resonator, also for the case of a nonlinear and a linear device. In all figures, for the nonlinear measurement resonator, when we set the coarse-graining value as $\sigma = 10$, the post-measurement state of the USC cavity and qubit changes significantly, depending on the measurement outcome, and so we observe a clear measurement backaction on the ultra-strongly coupled system. Interestingly, in these examples, we set the coupling strength J as approximately 300 times smaller than the qubit energy. On the other hand, for a linear resonator, the effect of the measurement backaction is negligible in this regime, and the post-measurement state is almost independent of the measurement results.

A. Low-energy two-level approximation

To give an intuitive explanation for why the nonlinear resonator can become strongly correlated with the USC system, even when the coupling strength is much smaller than the qubit energy, we introduce a two-level system approximation for the USC system. In our simulations, the initial state is $|G\rangle$, and the interaction Hamiltonian $J\hat{\sigma}_z b^\dagger b$ mainly induces a transition from $|G\rangle$ to the first excited state $|E\rangle = \frac{1}{\sqrt{2}}(|R\rangle|\alpha\rangle + |L\rangle|-\alpha\rangle)$. Since the transition matrix elements of the interaction Hamiltonian to the other excited states are negligible, we can approximate the low-energy states of the ultra-strongly coupled system as a two-level system. In this case, \hat{H}_{Rabi} and \hat{H}_{int} can be written as

$$\hat{H}_{\text{Rabi}} \approx \frac{\omega_{\text{eff}}}{2} \hat{\sigma}'_z \quad (17)$$

$$\hat{H}_{\text{int}} \approx J \hat{\sigma}'_x \hat{b}^\dagger \hat{b}, \quad (18)$$

where $\omega_{\text{eff}} = \omega_q \exp[-2\alpha^2]$, $\hat{\sigma}'_z = |E\rangle\langle E| - |G\rangle\langle G|$ and $\hat{\sigma}'_x = |G\rangle\langle E| + |E\rangle\langle G|$. In Fig. 6, we plot $\langle \hat{\sigma}'_x \rangle$ corresponding to $\hat{\rho}_{x \geq 0}$ and $\hat{\rho}_{x < 0}$, with this two-level system

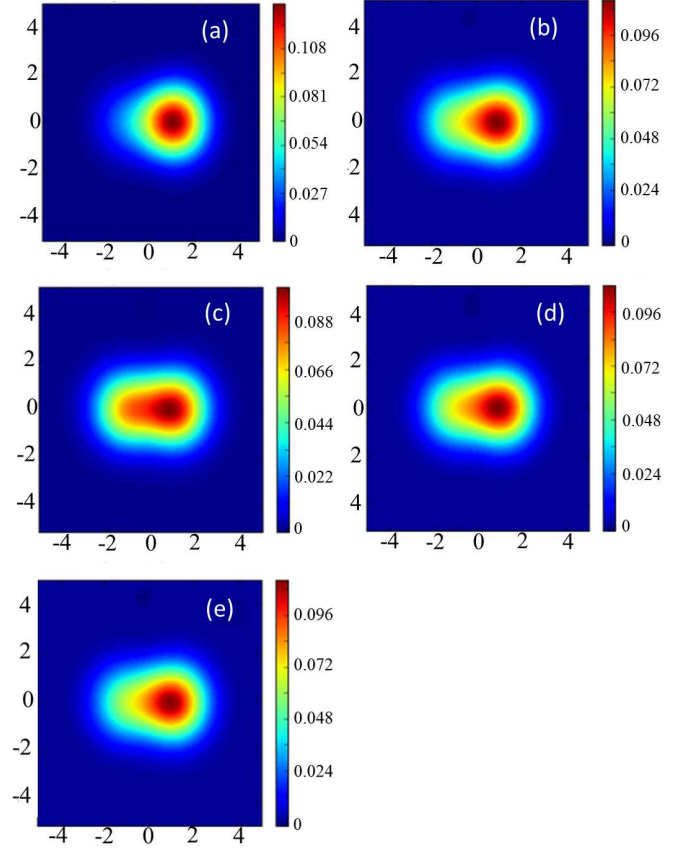


FIG. 2: (Color online) (a,b) The Q function of the reduced density matrix of the resonator ultra-strongly-coupled to the qubit after the coarse graining-measurement. We consider in (a) a projection into $x < 0$ at a time $t = 500$ ns for $\sigma = 0.5$, and (b) the same projection for $\sigma = 50$. Also, we show in (c) a projection into $x \geq 0$ at a time $t = 500$ ns for $\sigma = 0.5$ and (d) the same projection for $\sigma = 50$. For comparison, we plot in (e) the Q function at the time $t = 500$ ns just before the measurement of the nonlinear resonator is implemented. These examples confirm that, as we increase the value of σ , the change of the Q function induced by the measurement becomes smaller. We set $t = 500$ ns, $\omega_q = 2\pi \times 0.299$ GHz, $g = 2\pi \times 4.920$ GHz, $\omega_r = 2\pi \times 6.336$ GHz, $\kappa = 2\pi \times 2.375$ MHz, $\delta = 2\pi \times 5.698$ MHz, $\chi = 2\pi \times 80.735$ kHz, $f = 2\pi \times 22.792$ MHz, and $J = 2\pi \times 949.8$ kHz.

approximation. To check the validity of this simplified model, we plot $\hat{\sigma}'_x$ with this model in Fig. 6. These results show an excellent agreement with the results in Fig.4(a) based on the full Hamiltonian defined by Eq.(3)-(5).

With this two-level system approximation, we can show that the large correlation between the nonlinear resonator and the ultra-strongly-coupled system originates from the combination of an AC Stark shift and an adiabatic transition. It is easy to see that the large number of photons in the nonlinear resonator induces an energy shift (AC Stark shift) of the USC two-level system. Since

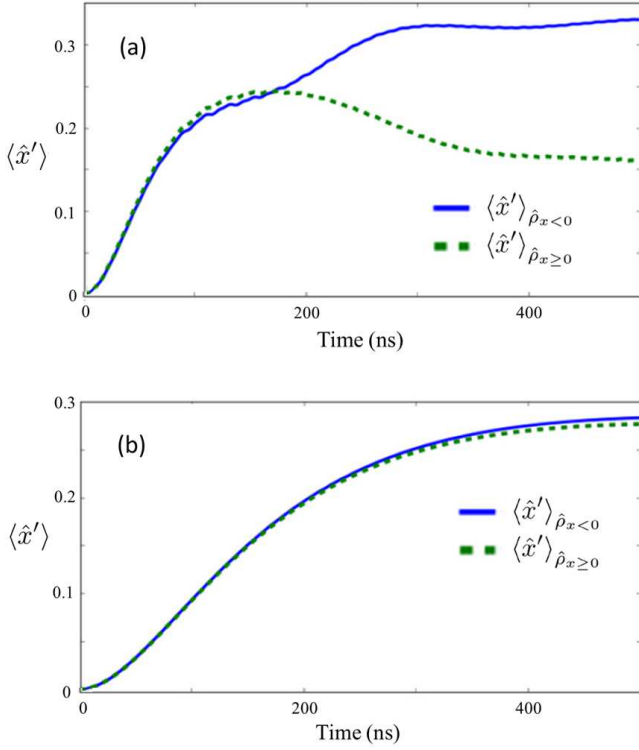


FIG. 3: (Color online) $\langle \hat{x}' \rangle$ after the coarse-graining measurement that projects the state into $\hat{\rho}_{x \geq 0}$ or $\hat{\rho}_{x < 0}$ depending on the measurement results. We plot the $\langle \hat{x}' \rangle$ in (a) with the nonlinear resonator and (b) with the linear resonator as the measurement apparatus. Here, we set the coarse-graining value as $\sigma = 5$. For the other parameters, we use the same as those in Fig. 2.

the photon number of the high-amplitude state is different from that of the low-amplitude state, the size of the AC Stark shift strongly depends on the state of the nonlinear resonator. As long as the timescale of the change in the nonlinear resonator photons is much smaller than $1/\omega_{\text{eff}}$, the state of the two-level system remains in a ground state of the following effective Hamiltonian

$$\hat{H}_{\text{eff}} = J \langle \hat{b}^\dagger \hat{b} \rangle_{H(L)} \hat{\sigma}'_x + \frac{\omega_{\text{eff}}}{2} \hat{\sigma}'_z, \quad (19)$$

where $\langle \hat{b}^\dagger \hat{b} \rangle_H$ ($\langle \hat{b}^\dagger \hat{b} \rangle_L$) is the average photon number of the high (low) amplitude state.

We expect that, when the nonlinear measurement resonator becomes a mixed state of the low- and high-amplitude states, the AC Stark shift (whose amplitude depends on the nonlinear resonator state) induces an adiabatic change of the ground state of the two-level system. This leads to the large correlation between USC system and measurement resonator. To show the validity of this interpretation, we analytically calculate the $\langle \hat{\sigma}'_{z(x)} \rangle$ of the ground state of the Hamiltonian in Eq. (19) where we substitute the numerically calculated photon numbers of the high (low) amplitude state for $\langle \hat{b}^\dagger \hat{b} \rangle_H$ ($\langle \hat{b}^\dagger \hat{b} \rangle_L$). In Fig. 7, we compare these results with the numerical sim-

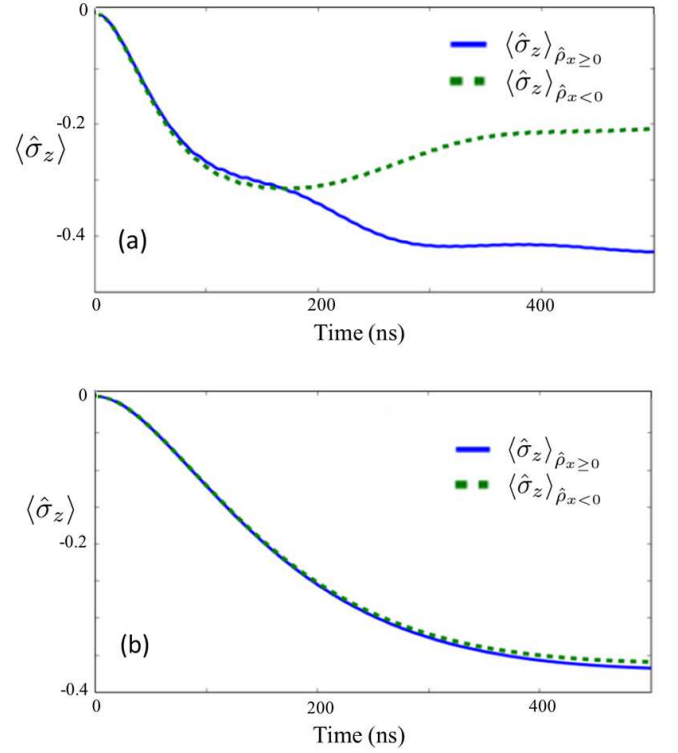


FIG. 4: (Color online) $\langle \hat{\sigma}_z \rangle$ after the coarse-graining measurements that projects the state into $\hat{\rho}_{x \geq 0}$ or $\hat{\rho}_{x < 0}$ depending on the measurement results. We plot $\langle \hat{\sigma}_z \rangle$ in (a) with the nonlinear resonator and in (b) with the linear resonator as the measurement apparatus. Here, we set the coarse-graining value as $\sigma = 5$. For the other parameters, we use the same as those in Fig. 2.

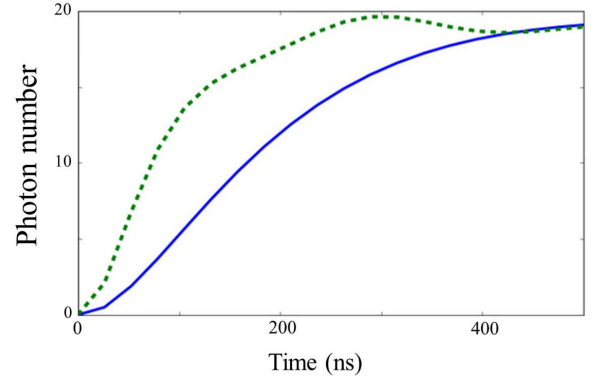


FIG. 5: (Color online) The average number of photons in the nonlinear resonator (dashed green curve) and in the linear resonator (blue continuous curve). The parameters used are the same as those in Fig. 3.

ulations [48, 49] where the master equation with the simplified Hamiltonian is solved. There is a good agreement between these two results, leading us to conclude that the correlation between the two-level system and the nonlinear resonator is induced by the described adiabatic

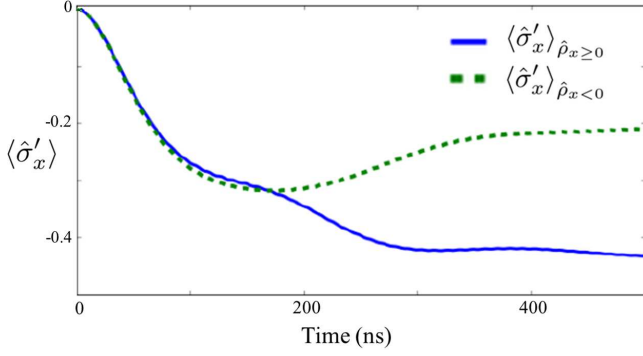


FIG. 6: (Color online) Numerical simulations of the expected values of $\hat{\sigma}'_x$ after the nonlinear resonator is projected into a high-amplitude state or a low-amplitude state. We use the same parameters as those in Fig. 4.

changes due to the AC Stark shift, whose amplitude depends on the nonlinear resonator state[53].

B. Comparison to QND limit

To compare our non-energy eigenbasis measurements with a ideal quantum non-demoliton (QND) measurements, we study the behavior of the the Q function of the nonlinear resonator, as shown in Fig. 8. Here, we consider the following four cases; (a) a non-energy eigenbasis measurement with the full Hamiltonian described in Eq. (4), (b) a non-energy eigenbasis measurement with the two-level system approximation described by the Eq. 19, (c) quantum non-demoliton measurements for the full Hamiltonian described in Eq. (4) in the limit $\omega_q = 0$ (which makes the measurement satisfy the QND condition $[\hat{H}_{\text{Rabi}}, \hat{H}_{\text{int}}] = 0$), and (d) null measurements with $J = 0$.

First, we again confirm that the two-level system approximation (b) compares well to the full Hamiltonian case (a). Moreover, we observe a clear difference between our non-energy eigenbasis measurements and measurements in the QND limit (c). In particular, the probability to obtain the high-amplitude state in the the nonlinear resonator becomes much larger for QND measurements than that for the the non-energy eigenbasis measurement case.

Second, a naive application of the rotating-wave approximation to the system and measurement device coupling term, for the non-energy eigenbasis measurement case, suggests the influence of system and measurement apparatus on each other should be entirely negligible. Of course, there is a clear difference between the case with a finite J and the case without J , because such an approximation should also take into account the norm of the operator in the interaction term, which for the driven nonlinear resonator can be large. The figures show that, roughly speaking, the probability to obtain

the high-amplitude state of the resonator for the non-energy eigenbasis measurements lies between the case of the QND measurements and null measurements.

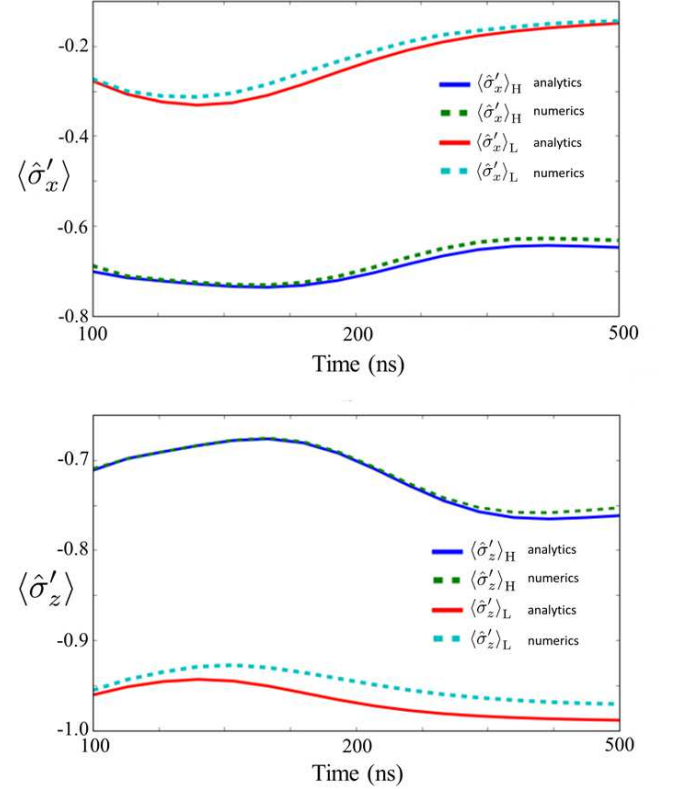


FIG. 7: (Color online) Numerical results and analytical solutions of the expected values of $\hat{\sigma}'_x$ and $\hat{\sigma}'_z$ after the nonlinear resonator is projected into a high-amplitude state or a low-amplitude state. In the analytical calculations, we use the simplified Hamiltonian described in the Eq. (19).

Also, we increase the ratio J/ω_q to check how the effect of the AC Stark shift will change. In Fig. 9(a), we plot $\langle \hat{\sigma}'_x \rangle_{\hat{\rho}_{x \geq 0}}$, $\langle \hat{\sigma}'_x \rangle_{\hat{\rho}_{x < 0}}$, and the Q function at $t = 500$ nm where the effective energy ω_{eff} is 10% that used in Fig.4. From the Fig. 9(a), the system converges into an eigenstate of $\hat{\sigma}'_x$ after the interaction, regardless of the measurement results of the nonlinear resonator. This can be understood by considering that the AC Stark effect $J(\hat{b}^\dagger \hat{b})_{\text{H(L)}}$ becomes much larger than the effective energy ω_{eff} so that the state of the ultra-strongly-coupled system becomes an eigenstate of $\hat{\sigma}'_x$ for both the high amplitude state and low amplitude state. Furthermore, it is worth mentioning that, from Fig. 9(b), the nonlinear resonator before the measurement almost becomes a high-amplitude state. For an ideal quantum projective measurements on the ground state of the ultra-strongly coupled system, the population in the low-amplitude state should be the same as that of the high-amplitude state, and so this result shows that the effective energy ω_{eff} is still too large to realize a full projective measurement in the persistent current basis.

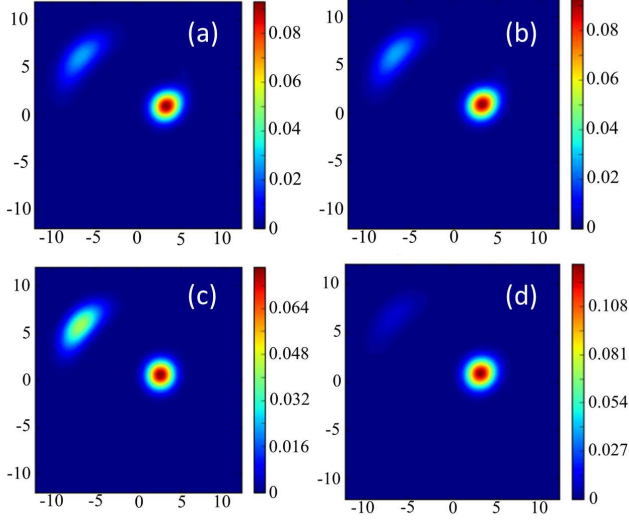


FIG. 8: (Color online) The Q functions of the nonlinear resonator for several conditions: (a) Numerical simulation of the full Hamiltonian described in Eq. (3)-(5). (b) The two-level system approximation. (c) Ideal QND measurement, which is possible in the limit $\omega_q = 0$. (d) When the nonlinear resonator does not couple at all with the qubit. We use the same parameters as those in Fig. 4.

We also consider a case when the effective energy ω_{eff} is 1% of that used in Fig. 4. In that case, $\langle \hat{\sigma}_z \rangle_{\hat{\rho}_{x < 0}}$ becomes much larger than $\langle \hat{\sigma}_z \rangle_{\hat{\rho}_{x \geq 0}}$, and this cannot be explained just by the AC Stark shift. Moreover, from Fig. 9(c), the population of the high-amplitude state becomes comparable with that of the low-amplitude state. Therefore, in this regime, we realize a strong projection of the ground state of the ultra-strongly-coupled system in the non-energy eigenbasis.

IV. NEGATIVITY

As a criteria of entanglement, and to understand how correlations between nonlinear resonator and USC system develop, we consider the negativity. Suppose there is a Hilbert space of two systems, $\mathcal{H}_A \otimes \mathcal{H}_B$ with a state $\hat{\rho}_{AB}$. The definition of negativity is

$$N(\hat{\rho}) = \frac{\|\hat{\rho}^{TA}\| - 1}{2} \quad (20)$$

here, $\hat{\rho}^{TA}$ is the partial transpose of the state $\hat{\rho}_{AB}$ taken over a subsystem A , and $\|\hat{X}\| = \text{Tr} \sqrt{\hat{X}^\dagger \hat{X}}$ is the trace norm [50]. In our case, the subsystem A corresponds to the two-level system approximation of the USC system, and B to the nonlinear resonator. In Fig. 10 we plot the negativity to quantify the entanglement between the ultra-strongly-coupled system and the nonlinear resonator. As we increase the ratio J/ω_q , the negativity also increases. These results show that a reasonably large

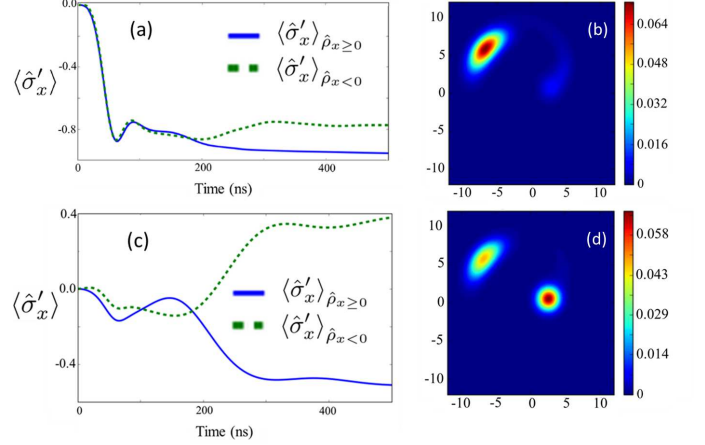


FIG. 9: (Color online) (a,b) Dynamics of the ultra-strongly-coupled system and the nonlinear resonator when the effective energy ω_{eff} is 10 times smaller than those in Fig. 4. (a) The expected value of $\hat{\sigma}'_x$ after the nonlinear resonator is projected into a high-amplitude state or a low-amplitude state. (b). The Q function of the nonlinear resonator at time 500 ns. (c,d) Dynamics of the ultra-strongly-coupled system and the nonlinear resonator when the effective energy ω_{eff} is 100 times smaller than those in Fig. 4. (c) The expected value of $\hat{\sigma}'_x$ after the nonlinear resonator is projected into a high-amplitude state or a low-amplitude state. (d). The Q function of the nonlinear resonator at time 500 ns. Except for the effective energy of the ultra-strongly coupled system, we use the same parameters as those in Fig 4.

entanglement between the ultra-strongly-coupled system and the nonlinear resonator is generated in the regime where we realize a projective measurement on the non-energy eigenbasis. However, due to the decoherence of the nonlinear resonator, the entanglement quickly degrades, and a classical correlation remains in these systems just before the measurement on the nonlinear resonator.

V. QUANTUM DISCORD

Finally, to elucidate the previous results further, we consider the quantum discord (QD), which is defined as follows. Two possible definitions of the mutual information of the state $\hat{\rho}_{AB}$

$$I(\hat{\rho}_{AB}) = S(\hat{\rho}_A) + S(\hat{\rho}_B) - S(\hat{\rho}_{AB}) \quad (21)$$

$$J_A(\hat{\rho}_{AB}) = S(\hat{\rho}_B) - S(\hat{\rho}_B | \hat{\rho}_A) \quad (22)$$

where $S(\hat{\rho})$ is a von Neumann entropy for a state $\hat{\rho}$, $\hat{\rho}_{A(B)}$ is a reduced density operator for $\mathcal{H}_{A(B)}$, and $S(\hat{\rho}_B | \hat{\rho}_A)$ is a quantum generalization of a conditional entropy. In the purely classical case, one can show that these two definitions of the mutual information are equivalent. However, in the nonclassical case, these definitions do not necessarily coincide. Also, $J_A(\hat{\rho}_{AB})$ is dependent on the measurement basis \hat{M}^A for \mathcal{H}_A . Therefore, QD is defined

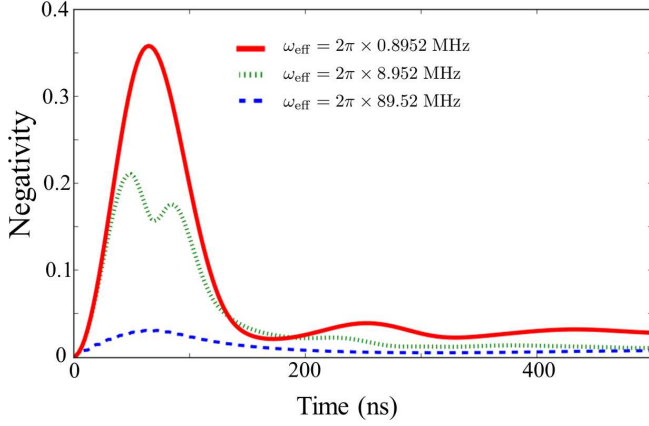


FIG. 10: (Color online) Entanglement between the ultra-strongly coupled system and the nonlinear resonator. We use the negativity as a measure of the entanglement. From the top, we plot the results with the effective energy of $\omega_{\text{eff}} = 2\pi \times 0.8952$ MHz, $\omega_{\text{eff}} = 2\pi \times 8.952$ MHz, and $\omega_{\text{eff}} = 2\pi \times 89.52$ MHz. Except for the effective energy of the ultra-strongly coupled system, we use the same parameters as those in Fig. 4.

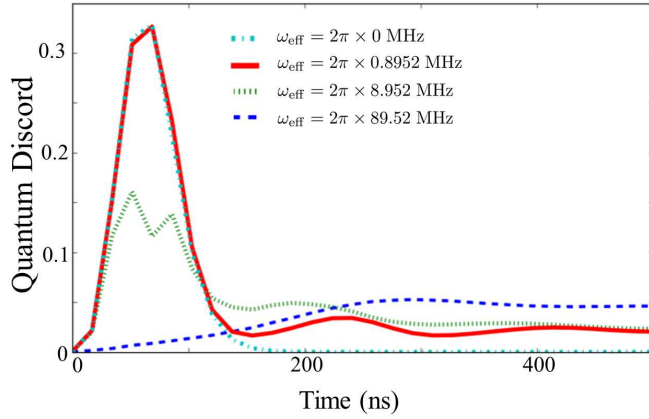


FIG. 11: (Color online) Quantum discord between the ultra-strongly coupled system and the nonlinear resonator. From the top, we plot the results with the effective energy of $\omega_{\text{eff}} = 2\pi \times 0$ MHz, $\omega_{\text{eff}} = 2\pi \times 0.8952$ MHz, $\omega_{\text{eff}} = 2\pi \times 8.952$ MHz, and $\omega_{\text{eff}} = 2\pi \times 89.52$ MHz. Except for the effective energy of the ultra-strongly coupled system, we use the same parameters as those in Fig. 4.

as

$$\mathcal{Q} = I(\hat{\rho}_{AB}) - \max_{\hat{M}^A} \{J_{\hat{M}^A}(\hat{\rho}_{AB})\} \quad (23)$$

$$= S(\hat{\rho}_A) - S(\hat{\rho}_{AB}) + \min_{\hat{M}^A} S(\hat{\rho}_{B|\{\hat{M}^A\}}) \quad (24)$$

where $S(\hat{\rho}_{B|\{\hat{M}^A\}}) = \sum_k p_k S(\hat{M}_k^A \hat{\rho}_{AB} \hat{M}_k^A / p_k)$, $p_k = \text{Tr}(\hat{M}_k^A \hat{\rho})$ (\hat{M}_k^A is a projector when the result is k), and QD is basis independent and reflects only non-classical correlation [51, 52]. In our case, system A corresponds to the approximated two level system and

system B the nonlinear resonator. We set the measurement basis on the approximated two level system as $\{|\varphi_1\rangle\langle\varphi_2|, |\varphi_2\rangle\langle\varphi_2|\}$, $|\varphi_1\rangle = \cos(\theta/2)|g\rangle + e^{i\phi}\sin(\theta/2)|e\rangle$, $|\varphi_2\rangle = \sin(\theta/2)|g\rangle - e^{i\phi}\cos(\theta/2)|e\rangle$ ($0 \leq \theta \leq \pi, 0 \leq \phi < 2\pi$) where $|e\rangle$ and $|g\rangle$ is the eigenstate of $\hat{\sigma}'_x$ and find (θ, ϕ) which realizes $\min_{\hat{M}^A} S(\hat{\rho}_{B|\{\hat{M}^A\}})$.

We plot QD in Fig. 11. Interestingly, in contrast to the negativity, QD, at $t = 500$ ns, becomes larger as J/ω_q is decreased. This can be explained in the following way: if J/ω_q is sufficiently large, the state becomes a highly entangled state well approximated by the form

$$\frac{1}{\sqrt{2}}(|e\rangle|Low\rangle - |g\rangle|High\rangle), \quad (25)$$

which decays, due the measurement of the nonlinear cavity, to the mixture

$$\hat{\rho}_f = \frac{1}{2}(|e\rangle\langle e| \otimes |Low\rangle\langle Low| + |g\rangle\langle g| \otimes |High\rangle\langle High|), \quad (26)$$

where $|High\rangle$ and $|Low\rangle$ are high and low amplitude states of the nonlinear resonator. Since $|e\rangle$ and $|g\rangle$ are orthogonal to each other, $\hat{\rho}_f$ is a classically correlated state without any superposition, implying vanishing QD. On the other hand, when J/ω_q is small, the dynamics can be explained by an AC Stark shift and the state can be expressed as

$$\begin{aligned} \hat{\rho}_a = & p_H |\psi_H\rangle\langle\psi_H| \otimes |High\rangle\langle High| \\ & + p_L |\psi_L\rangle\langle\psi_L| \otimes |Low\rangle\langle Low|, \end{aligned} \quad (27)$$

where $p_{L(H)}$ is the probability that the nonlinear resonator is in the low (or high) amplitude state. The state $|\psi_{H(L)}\rangle$ is the ground state of \hat{H}_{eff} . Here, $|\psi_H\rangle$ and $|\psi_L\rangle$ are not always orthogonal to each other, and as such the correlation in the mixture of the two could have a non-classical nature. Hence, the QD, in the long-time limit, tends to have a finite value when J/ω_q is small.

VI. CONCLUSIONS

In conclusion, we investigated quantum measurements in the ultra-strong-coupling regime of a light-matter system. In particular, we showed how the ground state of an ultra-strongly-coupled system can be measured by a nonlinear resonator. Interestingly, we found that, even if the coupling strength with the measurement device is two orders of magnitude smaller than the typical energy scale of the ultra-strongly-coupled system, we can still induce a strong classical correlation with the measurement device. Also, we confirmed that, by increasing the coupling strength with the measurement device, the entanglement between the system and measurement device can be generated, and we can realize projective measurements on the ground state of the ultra-strongly-coupled system. In addition, we found that the quantum discord tends to

have a finite value at large times in the regime when the dynamics can be described by AC Stark shift. Our results help illuminate the mechanism of how an ultra-strongly coupled system interacts with a measurement device.

Acknowledgments

We acknowledge helpful discussions with Roberto Stassi. This work was supported by JSPS KAKENHI Grants 15K17732 and MEXT KAKENHI Grant Num-

ber 15H05870. FN acknowledges support from CREST grant No. JPMJCR1676, the RIKEN iTHES Project, the MURI Center for Dynamic Magneto-Optics via the AFOSR award number FA9550-14-1-0040, the IMPACT program of JST, and a Grant-in-Aid for Scientific Research (A) and a grant from the Sir John Templeton Foundation.

-
- [1] M. Wallquist, K. Hammerer, P. Rabl, M. Lukin, and Zoller, P. Hybrid quantum devices and quantum engineering. *Phys. Scr.* **T137**, 014001 (2009).
 - [2] T. Duty, Towards superconductor-spin ensemble hybrid quantum systems. *Physics* **3**, 80 (2010).
 - [3] Z. Xiang, S. Ashhab, J.Q. You, and F. Nori, Hybrid quantum circuits: superconducting circuits interacting with other quantum systems, *Rev. Mod. Phys.* **85**, 623653 (2013).
 - [4] I. Buluta, S. Ashhab, and F. Nori, Natural and artificial atoms for quantum computation Reports on Progress in Physics **74**, 104401 (2011)
 - [5] I. Georgescu, F. Nori, Quantum technologies: an old new story, *Physics World* **25**, 16-17 (2012).
 - [6] X. Zhu, Y. Matsuzaki, R. Amsüss, K. Kakuyanagi, T. Shimo-Oka, N. Mizuochi, K. Nemoto, K. Semba, W. J. Munro and S. Saito, Observation of dark states in a superconductor diamond quantum hybrid system, *Nature Communications* **5**, 3424 (2014).
 - [7] K. Kakuyanagi, Y. Matsuzaki, C. Déprez, H. Toida, K. Semba, H. Yamaguchi, W. J. Munro, and S. Saito, Observation of Collective Coupling between an Engineered Ensemble of Macroscopic Artificial Atoms and a Superconducting Resonator, *Phys. Rev. Lett.* **117**, 210503 (2016).
 - [8] S. Ashhab and F. Nori. Qubit-oscillator systems in the ultrastrong-coupling regime and their potential for preparing nonclassical states, *Phys. Rev. A* **81**, 042311(2011).
 - [9] Y. Zhang, G. Chen, L. Yu, Q. Liang, J.-Q. Liang, and S. Jia, Analytical ground state for the Jaynes-Cummings model with ultrastrong coupling, *Phys. Rev. A* **83**, 065802 (2011).
 - [10] F. Beaudoin, J. M. Gambetta, and A. Blais, Dissipation and ultrastrong coupling in circuit QED, *Phys. Rev. A* **84**, 043832 (2011).
 - [11] S. Agarwal, S.M. Hashemi Rafsanjani and J.H. Eberly, Dissipation of the Rabi model beyond the rotating wave approximation: Quasi-degenerate qubit and ultra-strong coupling, *J. Phys. B.* **46**, 224017(2013).
 - [12] P. Nataf and C. Ciuti, Protected quantum computation with multiple resonators in ultrastrong coupling circuit QED, *Phys. Rev. Lett.* **107**, 190402 (2011)
 - [13] R. Stassi and F. Nori, Quantum Memory in the Ultrastrong-Coupling Regime via Parity Symmetry Breaking, *arXiv:1703.08951* (2017).
 - [14] K. Rzewski and K. Wodkiewicz, Phase Transitions, Two-Level Atoms, and the A^2 Term, *Phys. Rev. Lett.* **35**, 432 (1975).
 - [15] F. Yoshihara, T. Fuse, S. Ashhab, K. Kakuyanagi, S. Saito and K. Semba, Superconducting qubit-oscillator circuit beyond the ultrastrong-coupling regime, *Nature Physics* **13**, 4447 (2017).
 - [16] P. Forn-Daz, J. J. Garc a-Ripoll, B. Peropadre, J.-L. Orgiazzi, M. A. Yurtalan, R. Belyansky, C. M. Wilson and A. Lupascu, Ultrastrong coupling of a single artificial atom to an electromagnetic continuum in the nonperturbative regime, *Nature Physics* **13**, 3943 (2017).
 - [17] Z. Chen, Y. Wang, T. Li, L. Tian, Y. Qiu, K. Inomata, F. Yoshihara, S. Han, F. Nori, J. S. Tsai, and J. Q. You, Multi-photon sideband transitions in an ultrastrongly-coupled circuit quantum electrodynamics system, *arXiv:1602.01584* (2016).
 - [18] S. De Liberato, D. Gerace, I. Carusotto, and C. Ciuti, Extracavity quantum vacuum radiation from a single qubit, *Phys. Rev. A* **80**, 053810, (2009).
 - [19] J.R. Johansson, G. Johansson, C.M. Wilson, and F. Nori, Dynamical Casimir effect in a superconducting coplanar waveguide, *Phys. Rev. Lett.* **103**, 147003 (2009).
 - [20] J.R. Johansson, G. Johansson, C.M. Wilson, and F. Nori, Dynamical Casimir effect in superconducting microwave circuits, *Phys. Rev. A* **82**, 052509 (2010).
 - [21] C.M. Wilson, G. Johansson, A. Pourkabirian, J.R. Johansson, T. Duty, F. Nori, and P. Delsing, Observation of the dynamical Casimir effect in a superconducting circuit, *Nature* **479**, 376 (2011).
 - [22] P.D. Nation, J.R. Johansson, M.P. Blencowe, F. Nori, Stimulating uncertainty: Amplifying the quantum vacuum with superconducting circuits, *Rev. Mod. Phys.* **84**, 1-24 (2012).
 - [23] J.R. Johansson, G. Johansson, C.M. Wilson, P. Delsing, F. Nori, Nonclassical microwave radiation from the dynamical Casimir effect, *Phys. Rev. A* **87**, 043804 (2013).
 - [24] R. Stassi, A. Ridolfo, O. Di Stefano, M.J. Hartmann and S. Savasta, Spontaneous conversion from virtual to real photons in the ultrastrong-coupling regime, *Phys. Rev. Lett.* **110**, 243601, (2013).
 - [25] M. Cirio, S. De Liberato, N. Lambert, and F. Nori, Ground State Electroluminescence, *Phys. Rev. Lett.* **116**, 113601, (2016).
 - [26] M. Cirio, K. Debnath, N. Lambert, F. Nori, *arXiv preprint, arXiv:1612.02953* (2016).
 - [27] J. Lolli, A. Baksic, D. Nagy, V. E. Manucharyan, and C.

- Ciuti, Ancillary Qubit Spectroscopy of Vacua in Cavity and Circuit Quantum Electrodynamics, *Phys. Rev. Lett.* **114**, 183601 (2015).
- [28] S. Ashhab, J.Q. You, and F. Nori, Weak and strong measurement of a qubit using a switching-based detector, *Phys. Rev. A* **79**, 032317 (2009).
- [29] S. Ashhab, J.Q. You, and F. Nori, The information about the state of a qubit gained by a weakly coupled detector, *New J. Phys.* **11**, 083017 (2009).
- [30] S. Ashhab, J.Q. You, F. Nori, The information about the state of a charge qubit gained by a weakly coupled quantum point contact, *Phys. Scr. T* **137**, 014005 (2009).
- [31] K. Kakuyanagi, T. Baba, Y. Matsuzaki, H. Nakano, S. Saito and K. Semba, Observation of quantum Zeno effect in a superconducting flux qubit, *New J. Phys.* **17** (2015).
- [32] K. Kakuyanagi, Y. Matsuzaki, T. Baba, H. Nakano, S. Saito, K. Semba, Characterization and Control of Measurement-Induced Dephasing on Superconducting Flux Qubit with a Josephson Bifurcation Amplifier. *J. Phys. Soc. Jpn.* **85**, 104801 (2016).
- [33] I. Siddiqi, R. Vijay, F. Pierre, C. M. Wilson, M. Metcalfe, C. Rigetti, L. Frunzio, and M. H. Devoret, RF-Driven Josephson Bifurcation Amplifier for Quantum Measurement, *Phys. Rev. Lett.* **93**, 207002 (2004).
- [34] I. Siddiqi, R. Vijay, M. Metcalfe, E. Boaknin, L. Frunzio, R. J. Schoelkopf, and M. H. Devoret, Dispersive measurements of superconducting qubit coherence with a fast latching readout, *Phys. Rev. B* **73**, 054510 (2006).
- [35] A. Lupascu, S. Saito, T. Picot, P. C. de Groot, C. J. P. M. Harmans and J. E. Mooij, Quantum non-demolition measurement of a superconducting two-level system, *Nature Physics* **3**, 119 - 125 (2007).
- [36] N. Boulant, G. Ithier, P. Meeson, F. Nguyen, D. Vion, D. Esteve, I. Siddiqi, R. Vijay, C. Rigetti, F. Pierre, and M. Devoret, Quantum nondemolition readout using a Josephson bifurcation amplifier, *Phys. Rev. B* **76**, 014525 (2007).
- [37] K. Kakuyanagi, S. Kagei, R. Koibuchi, S. Saito, A. Lupascu, K. Semba and H. Nakano, Experimental analysis of the measurement strength dependence of superconducting qubit readout using a Josephson bifurcation readout method, *New J. Phys.* **15** (2013).
- [38] M. O. Scully and M. S. Zubairy, *Quantum Optics* (Cambridge University Press, Cambridge, 1997).
- [39] M. Rigo, G. Alber, F. Mota-Furtado and P. F. O'Mahony, Quantum-state diffusion model and the driven damped nonlinear oscillator, *Phys. Rev. A* **55**, 1665 (1997).
- [40] H. Nakano, S. Saito, K. Semba and H. Takayanagi, Quantum Time Evolution in a Qubit Readout Process with a Josephson Bifurcation Amplifier, *Phys. Rev. Lett.* **102**, 257003 (2009).
- [41] C. Laflamme and A. A. Clerk, Quantum-limited amplification with a nonlinear cavity detector, *Phys. Rev. A* **83**, 033803 (2011).
- [42] C. Laflamme and A. A. Clerk, Weak Qubit Measurement with a Nonlinear Cavity: Beyond Perturbation Theory, *Phys. Rev. Lett.* **109**, 123602 (2012).
- [43] M. Boissonneault, A. C. Doherty, F. R. Ong, P. Bertet, D. Vion, D. Esteve and A. Blais, Back-action of a driven nonlinear resonator on a superconducting qubit, *Phys. Rev. A* **85**, 022305 (2012).
- [44] C. Gardiner and P. Zoller, *Quantum Noise* (Springer, 2004).
- [45] A. Ridolfo, M. Leib, S. Savasta, and M. J. Hartmann, Photon Blockade in the Ultrastrong Coupling Regime, *Phys. Rev. Lett.* **109**, 193602 (2012).
- [46] L. Garziano, A. Ridolfo, R. Stassi, O. Di Stefano, and S. Savasta, Switching on and off of ultrastrong light-matter interaction: Photon statistics of quantum vacuum radiation, *Phys. Rev. A* **88**, 063829 (2013).
- [47] R. Stassi, S. Savasta, L. Garziano, B. Spagnolo and F. Nori, Output field-quadrature measurements and squeezing in ultrastrong cavity-QED, *New J. Phys.* **18**, 123005 (2016).
- [48] J.R. Johansson, P.D. Nation, and F. Nori, QuTiP 2: A Python framework for the dynamics of open quantum systems, *Comp. Phys. Comm.* **184**, 1234 (2013).
- [49] J.R. Johansson, P.D. Nation, and F. Nori, QuTiP: An open-source Python framework for the dynamics of open quantum systems, *Comp. Phys. Comm.* **183**, 1760 (2012).
- [50] An introduction to entanglement measures, MB Plenio, S Virmani, arXiv preprint, quant-ph/0504163, (2005).
- [51] H. Ollivier and W. H. Zurek, Quantum Discord: A Measure of the Quantumness of Correlations, *Phys. Rev. Lett.* **88**, 017901 (2001).
- [52] L. Henderson and V. Vedral: Classical, quantum and total correlations, *J. Phys. A* **34**, 6899 (2001).
- [53] In Fig. 7 we do not show the time evolution from $t = 0$ ns to $t = 100$ ns, because the high-amplitude state is not generated until approximately $t = 100$ ns.